Lorentz force effects on the electron energy distribution in inductively coupled plasmas

V. A. Godyak and B. M. Alexandrovich
OSRAM SYLVANIA, Beverly, Massachusetts 01915

V. I. Kolobov
CFD Research Corporation, Huntsville, Alabama 35805

(Received 27 March 2001; published 20 July 2001)

Depletion of the electron energy distribution function by slow electrons in the skin layer has been observed in experiment in a cylindrical inductive discharge with a flat coil at low frequency and low gas pressure. The origin of the effect lies in the dependence of the ponderomotive force (caused by the rf magnetic field) on the electron thermal motion under conditions of the anomalous skin effect. Analysis of the electron energy distribution based on the existence of adiabatic invariants for collisionless electron motion at low frequencies reveals enhanced anisotropy and time dependence of the electron distribution function due to strong rf magnetic fields and a polarization electrostatic potential at twice the driving frequency. The electron energy distributions calculated in the skin layer using experimentally measured electromagnetic fields and rf and dc potential profiles are in reasonable agreement with the experimental electron distributions.

DOI: 10.1103/PhysRevE.64.026406 PACS number(s): 52.80.−s, 52.65.−y

I. INTRODUCTION

Inductively coupled plasmas (ICPs) are widely used for semiconductor processing and lighting technology. In these applications, ICPs are produced in a variety of gas mixtures at pressures between a fraction of a mTorr and hundreds of mTorr in chambers with characteristic sizes 1–10 cm using both continuum and pulsed power operating regimes. The ICPs have been driven over a wide range of frequencies varying from tens of Hz to tens of mHz [1]. At low frequencies, ferromagnetic cores have to be used to enhance the magnetic field. A wide variety of sources with different coil geometry have been developed including cylindrical spiral and stove top planar coils driven at single or multiple frequencies. Multicoil ICPs are being developed to maintain a spatially uniform plasma over large surfaces.

The physics of an ICP has been a subject of active research in both industry and academia. It has been demonstrated that at low gas pressure, the electron kinetics can be adequately described in terms of the total electron energy $\varepsilon = w + eU_e$ (the sum of the kinetic energy w and the potential energy in the dc electrostatic field eU_e). Due to the very small energy loss in elastic collisions of electrons with heavy neutrals, the total electron energy is an approximate invariant of the electron motion. Thus, in low pressure discharges, the electron energy probability function (EEPF) f_0 depends solely on the total electron energy and EEPFs, measured at different spatial positions, coincide with each other when shifted by the local value of the electrostatic potential [2–4]. This EEPF feature (referred as nonlocal kinetics) has been observed in numerous experiments in capacitive and inductive rf discharges [5–12]. As a rule, the EEPFs deviate from Maxwellian and often exhibit a complex structure depending on the nature of the working gas and on specifics of the electromagnetic field interaction with electrons. In an ICP, due to the relatively high degree of ionization, the body of the EEPF corresponding to electrons with energy less than the excitation energy ε^* (the elastic energy range) is often a Maxwellian distribution owing to Coulomb interactions among electrons. In the inelastic energy range ($\varepsilon > \varepsilon^*$) the EEPF can be depleted compared to a Maxwellian distribution due to electron energy loss in excitation, ionization, and (at the lowest gas pressure) due to the escape of fast electrons to the wall.

The main interaction of the electromagnetic field with the plasma in inductive discharges takes place in the skin layer of thickness δ near the plasma boundary. Depending on gas pressure, plasma density, and driving frequency, the interaction of an electromagnetic field with plasma within the skin layer can be local or nonlocal in nature. The collisional (or/and very high frequency) regime, when electrons pass through the skin layer with many collisions and/or spend many rf field periods there [$v_{th}/\delta < (\omega^2 + \nu_{ea}^2)^{1/2}$], is the domain of Joule heating and normal skin effect, where $v_{th} = (2T_e/m)^{1/2}$ is the electron thermal velocity and ν_{ea} is the electron-atom collision frequency. The nearly collisionless regime when $v_{th}/\delta > (\omega^2 + \nu_{ea}^2)^{1/2}$ is the domain of nonlocal electrodynamics, anomalous skin effect [13], and collisionless electron heating [14,15]. Under the conditions of the anomalous skin effect, the current induced by the rf electric field is not determined solely by the local value of the rf field at that point, but depends also on the field profile in the neighborhood of the point [16].

Several hot plasma effects have been discovered recently in weakly collisional ICPs, including nonmonotonic field profiles [17] collisionless power dissipation [18–21], negative power absorption [22], etc. Peculiarities of collisionless heating result in a specific frequency dependence of the EEPF in the weakly collisional regime [23]. Static magnetic fields of only a few Gauss may result in a significant modification of the rf field penetration into the plasma [24]. Weak static magnetic fields can change the electron heating in an ICP [25] and influence the shape of the EEPF [26].

Trends towards lower operating frequency are clearly recognizable in recent ICP developments [27–29]. Low frequency operation reduces capacitive coupling and the trans-

mission line effect in ICP inductors and leads to simplification and lower cost of rf power sources and matching circuits. Scaling ICP sources to larger dimensions is also simplified at low frequencies. The transition to lower operating frequencies enriches the ICP physics due to enhancement of nonlinear interactions between electromagnetic fields and plasma electrons that are usually unimportant at the standard industrial frequency 13.56 MHz.

Nonlinear effects in ICP are mainly caused by the rf Lorentz force $\mathbf{F_L}=en[\mathbf{v}\times\mathbf{B}]$ acting on electrons in the skin layer. They bring about a variety of new phenomena discussed in recent literature, including generation of the second harmonic of the electrostatic potential [30] and rf current [31,32], and ponderomotive force effects on the spatial distribution of plasma density and the ambipolar potential [33]. It has been shown [33] that ponderomotive effects in an ICP are much smaller than those given by classical formula and that a significant ponderomotive effect is possible only under conditions of the anomalous skin effect.

A lower driving frequency results in augmentation of the Lorentz force produced by an rf magnetic field. At frequencies below 1 MHz, the Lorentz force can be much larger than the electric force produced by the induced electric field [33]. In an ICP, the Lorentz force is mainly directed normal to the plasma boundary and has a time-independent component and an oscillating component at twice the driving frequency. The time-independent component represents a ponderomotive (Miller) force that pushes electrons and ions out of the skin layer. This force can be described in terms of a ponderomotive potential U_p, ($\mathbf{F_p}=-en\nabla U_p$). By adding this potential to the electrostatic (ambipolar) potential, one can expect that the EEPF becomes a function of the new total electron energy, $f_0=f_0(w,U_e,U_p)$. In a macroscopic sense, this corresponds to a ponderomotive modification of the plasma density n and electrical (ambipolar) potential U_e, demonstrated recently for a low pressure, low frequency ICP [33]. In this paper we present results of an experimental and theoretical study of EEPFs in a low pressure ICP at low driving frequencies where substantial deviations from the ''usual'' EEPF behavior are observed in the skin layer.

II. EXPERIMENTAL SETUP AND MEASUREMENT TECHNIQUE

The EEDF measurements were carried out in a cylindrical ICP chamber (20 cm in diameter and 10.5 cm in length) with a quartz window and a planar induction coil shown in Fig. 1 and described in detail in Ref. [34]. The measurements were made in an ICP driven at $\omega/2\pi=0.45$ and 0.9 MHz in argon at a pressure of 1 mTorr where nonlinear phenomena are well expressed. For comparison, similar measurements were done for 3.39 and 6.78 MHz where nonlinear effects on the EEPF were negligible. The discharge power dissipated in the plasma was found by accounting for losses in the inductor coil and the matching circuit [34]. The discharge power was kept constant in these experiments at a level of 200 W. The ICP inductor coil and matching circuit were somewhat different for low frequencies (0.45 and 0.9 MHz) and for high frequencies (3.39 and 6.78 MHz). For all frequencies, the

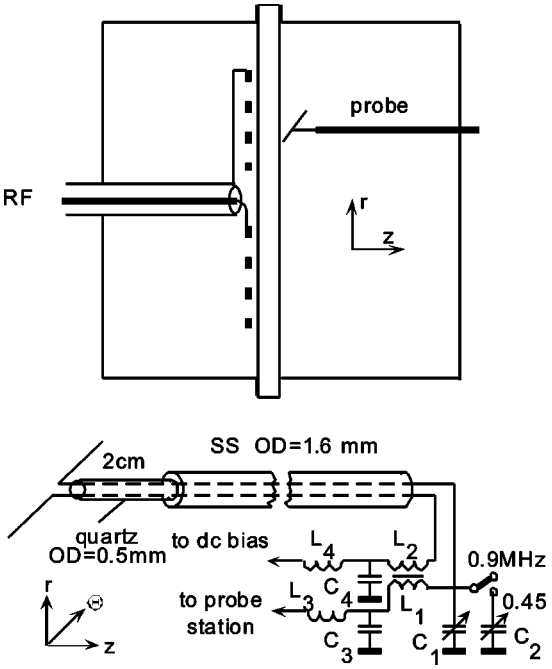

FIG. 1. Experimental ICP chamber and rf compensated probe circuitry.

induction coil had the same geometry and dimensions (3.8 cm ID and 12.7 cm OD), and was placed at the same distance from the window. For low operating frequency, the coil consisted of 20 turns of litz wire, while for high operating frequency the coil had only five turns as described in Ref. [34].

Langmuir probe measurements of the EEPF have been carried out in this ICP along its axial direction at the discharge axis ($r=0$) and at a fixed radial position ($r=4$ cm) corresponding to maxima in the radial distributions of the radial rf magnetic field, $B_{r\omega}(r)$ and the radial distributions of the azimuthal rf electric field, $E_{\theta\omega}(r)$. The measurements were made using our Langmuir probe station [35]. Low frequency noise suppression, probe circuit resistance compensation, ensemble averaging, and digital processing with adaptive filtering were implemented there to achieve high quality EEPF measurements. The basic plasma parameters, plasma density n, effective electron temperature T_e, and electron-atom collision frequency ν_{ea} were found as corresponding integrals of the EEPF. Additionally, a two-dimensional differential magnetic probe [17,36] was used to evaluate the axial distributions of the azimuthal rf electric field $E_{\theta\omega}(z)$ and the current density $J_{\theta\omega}(z)$ at a fixed radial position, $r=4$ cm.

Since capacitive coupling was negligible in low frequency operation, no electrostatic screen between the coil and plasma was needed to attain a low rf plasma potential relative to the ground. The measurement of rf plasma potential V_{rf} in the plasma [34] showed that for high frequencies (3.39–13.56 MHz), V_{rf} was much smaller than the electron temperature T_e. But at low operating frequencies, considerable oscillations of the electrostatic potential in the skin layer were observed [30], with the second harmonic potential $V_{2\omega}$ (shown in Fig. 2) being two orders of magnitude larger than the fundamental and all other harmonics. However, in the

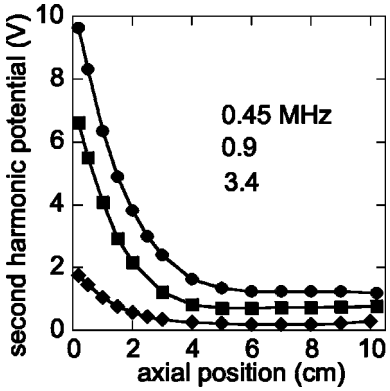

FIG. 2. Polarization rf potential $V_{2\omega}$ in the skin layer [30].

bulk plasma, far away from the skin layer, $V_{2\omega}$ was much smaller than the electron temperature ($T_e=6-7$ eV) and there was no need to rf compensate the probe to obtain undistorted probe measurements outside the skin layer.

Since the large gradient of $V_{2\omega}$ in the skin layer much exceeded the azimuthal rf electric field [30], it was impossible to achieve rf compensation of the probe with traditional means [35,37]. A relatively large floating electrode needed for rf shunting of the measurement probe would result in unacceptable distortion of the rf field and rf current in the skin layer. To solve this specific problem we developed a rf compensated double probe and corresponding circuitry shown in Fig. 1. Drastic reduction in the impedance of the shunting electrode (probe) relative to plasma [about $(m/M)^{1/2}$ times, where m and M are the electron and ion masses] was achieved by biasing it positively. This allowed for a significant reduction of the shunting electrode to the size of the small Langmuir probe.

The probe system shown in Fig. 1 consists of two equal thin cylindrical tungsten wires ($l_p=5$ mm, $r_p=0.05$ mm) oriented in the plane of constant z and directed along azimuthal rf electric field $E_{\theta\omega}$. Both probes are fitted to a quartz two-bore capillary having outer diameter of 0.5 mm and extended length of 2 cm. The capillary is built into a stainless steel tube shaft having diameter of 1.6 mm, in the discharge chamber and 6.35 mm outside the chamber, and fixed on a vacuum-sealed moving stage allowing axial displacement of the probe. It is imperative to keep the probe holder (quartz capillary and shaft part penetrating the plasma) as thin as possible to minimize local and global plasma disturbance. At the end of the probe shaft (outside the discharge chamber) the probe leads were sealed in epoxy and connected to a metal filter box containing a two-channel resonant transformer filter (shown in Fig. 1) tuned to the second harmonic of the driving frequency, 2ω. After the filter, the probe leads were connected, respectively, to a dc bias voltage source and to the probe station.

The probe system operates as following. One of the probe wire works as a measuring Langmuir probe, while the second serves as a shunting probe equalizing the rf potential of the measuring probe to the plasma rf potential V_{rf}. That is achieved by biasing the reference probe to the dc plasma potential (where probe resistance to plasma is minimal and its coupling to plasma is maximal) and by inductive coupling the two probes with a 1:1 resonant transformer as shown in Fig. 1. The transformer consists of two bifilar windings (having inductances L_1 and L_2) on a ferrite pot core and, therefore, provides an ideal coupling between L_1 and L_2 (the rf voltage across each winding is equal to each other). Thus, for rf signal, both windings work in parallel as a single coil with inductance $L=L_1=L_2$. Being resonant with capacitors C_1 and C_3, C_4 and the probe wires capacitance C_p to the grounded probe shaft ($C_3=C_4\gg C_1\approx C_p$), this inductance forms a resonant tank filter with its resistance $R_f\approx 2Q\omega L$; where Q is the Q factor of the resonant circuit. In our experiment R_f was about 380 and 520 kΩ, corresponding to 0.45 and 0.9 MHz, while the impedance of the shunting probe R_{po} for the lowest plasma density in the skin layer ($n_{min}\approx 3\times 10^{10}$ cm^{-3}) was about 20 kΩ. In the worst case of the largest rf plasma potential ($V_{rf}\approx 10$ V) and the smallest filter resistance R_f, the rf voltage in the sheath of the measuring probe, $V_{sh}=V_{rf}R_{po}/(R_f+R_{po})=0.5$ V, which was negligibly small compared with the electron temperature measured in the skin layer, $T_e=7$ eV. Thus, the condition of an EEDF measurement, undistorted by rf voltage $V_{sh}<0.3T_e/e$, [37,38], was met in this experiment. Here and throughout the paper we use rms values for all oscillatory quantities.

III. EXPERIMENTAL RESULTS AND DISCUSSION

Prior to discussing experimental results, let us briefly describe specific features of our ICP at a low operating frequency. At 1 mTorr the discharge is close to the ion free path regime ($\lambda_i>L,R$) with an electron mean free path λ_e being much larger than the chamber length L and radius R. At this condition the ICP operates in a strongly nonlocal regime (anomalous skin effect). Due to the low driving frequency, plasma screening has little effect on the electromagnetic field distribution, which is mainly defined by the chamber geometry. The electromagnetic field distribution with plasma is similar to that in vacuum with characteristic scale for the field decay $\delta\approx\delta_0=2.42$ cm$\approx R/3.83=2.61$ cm, corresponding to the rf electric field distribution in the vacuum chamber [14,39]. Here δ_0 is the characteristic length of the electric field decay in empty chamber. At 200 W and 1 mTorr, the plasma density and electron temperature in the plasma center ($r=0$, $z=5$ cm) were 1.3×10^{11} cm^{-3} and 6 eV, respectively. These same parameters in the middle of the plasma active zone ($r=4$ cm, $z=1$ cm) were about 5×10^{10} cm^{-3} and 7 eV, respectively. From magnetic probe measurements we found that $\omega_B^2\gg\omega^2+\nu_{ea}^2$ in the skin layer [33,40,41], where $\omega_B=eB_\omega/m$ is the electron cyclotron frequency and B_ω is the dominant (radial) component of rf magnetic field in the skin layer. This means that the nonlinear Lorentz force $\mathbf{F_L}=en[\mathbf{v}_\omega\times\mathbf{B}_\omega]$ greatly exceeds the electric force $\mathbf{F_E}=en\mathbf{E}_\omega$, where $\mathbf{v}_\omega$ is the electron rf drift velocity. Thus, under conditions of our experiment, the skin effect in the ICP was not only anomalous but also nonlinear [15,32,33,40,41].

The electron energy distributions measured at the axial position of maximal plasma density and in the middle of the skin layer ($z=1$ cm from the window), at a fixed radial

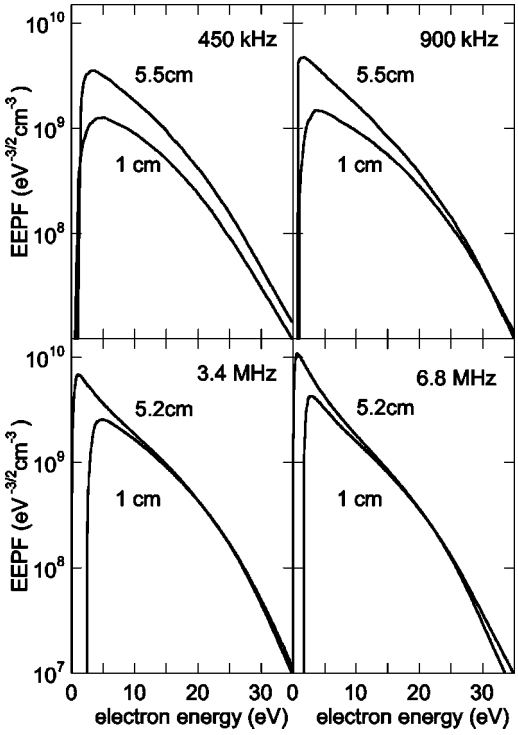

FIG. 3. EEPF measured for 0.45, 0.9, 3.39 and 6.78 MHz at the position of maximum plasma density ($z=z^*, r=4$ cm) and in the skin layer ($z=1$ cm, $r=4$ cm).

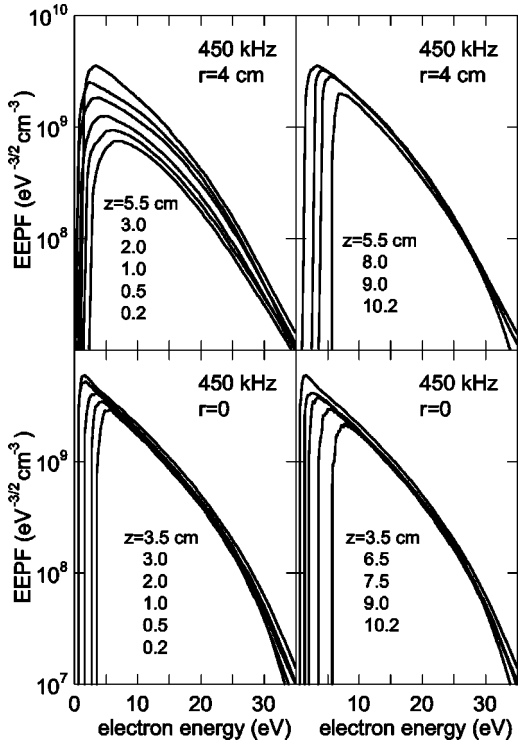

FIG. 4. Axial evolution EEPF at different radial positions for 0.45 MHz.

position ($r=4$ cm) are shown in Fig. 3 for different frequencies. The electron energy distribution is given in terms of the EEPF, $f_0(\varepsilon)$ plotted against the total electron energy $\varepsilon = w + eU_e$. The EEPF as a function of the electron kinetic energy $f_0(w)$ is proportional to the measured second derivative of the probe characteristic $I_p(V)$, $f_0(w) \propto d^2 I_p / dV^2$. The plasma potential is defined as the probe potential where the second derivative of the probe characteristic crosses zero.

As seen in Fig. 3, the shapes of EEPFs in the elastic energy range ($\varepsilon < \varepsilon^*$), measured at $r=4$ cm, in the point of the maximum plasma density, evolve from concave at high frequency (with a low energy peak) to convex at low frequency. The EEPFs measured at $r=0$ for low frequencies (not shown here) are essentially Maxwellian in the elastic energy range. An enhancement of the EEPF at low electron energy at high frequency is a result of nonlocal electron kinetics specific to electron interactions with electromagnetic fields under conditions of the anomalous skin effect analyzed in [23]. At lower frequency, more low energy electrons participate in the heating process in the skin layer resulting in higher temperature and the disappearance of the low energy peak in the EEPF.

In the inelastic energy range ($\varepsilon > \varepsilon^*$) the EEPF slope increases starting at about 20 eV. A depletion of the EEPF with high energy electrons is due to ionization and fast electron escape to the chamber walls whose potential is about 24 V lower than the plasma potential. Such an EEPF structure in inelastic energy range is typical for dc and rf discharges in the Tonks-Langmuir regime ($\lambda_i > R, L$) when direct ionization and escape to the wall are the major channels of fast electron loss. At higher pressure and/or larger chamber size (for our experimental device, at argon pressure about 10 mTorr and higher), the EEPF depletion starts when the electron energy is close to the excitation energy ε^*.

The EEPF measured at 3.39 and 6.78 MHz in different spatial positions (thus, at different plasma potential U_e) closely coincide for $\varepsilon > eU_e$ and $\nabla f_0(\mathbf{r}, \varepsilon) \approx 0$. This is a very common feature of bounded gas discharge plasmas at low gas pressure when the electron energy relaxation length is much larger than plasma size and is a consequence of nonlocal electron kinetics [2–4]. A small divergence in $f_0(\mathbf{r}, \varepsilon)$ in the vicinity of plasma potential (small electron kinetic energy) measured close to the window is typical for probe measurements at the ICP plasma boundary where a strong rf field is present, and is probably caused by relatively large directed velocity of low energy electrons v_ω approaching their thermal velocity.

A different EEPF evolution in the skin layer is seen in Fig. 3 for low driving frequencies 0.45 and 0.9 MHz. Here a significant difference is found for EEPFs measured at different positions, although the plasma potential difference between them is negligibly small, while the corresponding potential difference for both 3.39 and 6.78 MHz is about 2.0 V. Note that the EEPFs corresponding to the maximum plasma density, measured at low frequencies are shifted from $\varepsilon = 0$, while the EEPFs measured at high frequencies begin from $\varepsilon = 0$. This suggests that at low frequencies the maximum plasma density does not coincide with the minimum in the potential energy $eU_e = 0$.

Shown in Fig. 3, the EEPFs measured at low frequencies

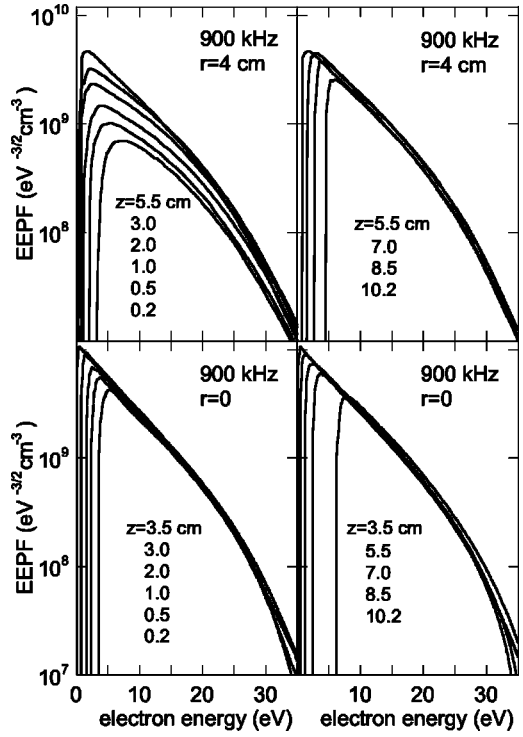

FIG. 5. Axial evolution EEPF at different radial positions for 0.9 MHz.

look as if they were heavily distorted by the rf voltage across the probe sheath. But the rf filtering in the probe circuit was thoroughly addressed in this experiment and the probe rf voltage was much less than that needed for undistorted EEPF measurement. Note rf probe distortion usually affects the EEPF in the vicinity of the plasma potential and does not change the slope of the EEPF for medium and high electron energies. However, the EEPFs measured in the skin layer at low frequencies diverge over a wide range of electron energies, although the divergence is largest for low energy electrons.

The EEPFs measured along axial direction at $r=4$ cm and on the discharge center ($r=0$) are shown in Figs. 4 and 5, correspondingly, for 0.45 and 0.9 MHz. Here, the EEPFs measured between the active plasma boundary ($z=0.2$ cm) and the position of maximum plasma density ($z=z^*$) are given on the left side, while the EEPFs measured between z^* and the point $z=9.2$ cm, near the passive plasma boundary, are given on the right side. The EEPF divergence takes place only in the area of large electromagnetic field ($r=4$ cm and $z<z^*$), while at $z>z^*$ and everywhere on the discharge central axis ($r=0$), where there is no electric field, the EEPFs measured at different positions and plasma potentials, coincide with each other. Similar measurements at high frequencies (see Fig. 6) did not show a considerable EEPF divergence in the skin layer, although the rf field there was larger than that at low frequencies. Measurements at lower discharge power showed an even larger divergence of EEPFs measured within the skin layer although the rf field in the skin layer was somewhat smaller at low power. This is shown in Fig. 7 for ICP at 50 W and 0.9 MHz. The weaker divergence at high discharge power (high plasma

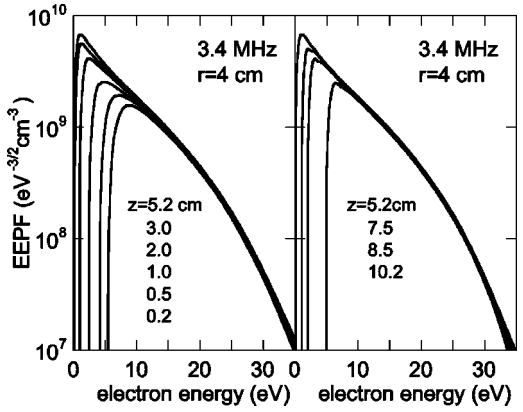

FIG. 6. Axial evolution EEPF at $r=4$ cm for 3.39 MHz.

density) could be explained by enhanced electron-electron collisions ($\nu_{ee} \propto n$) leading to EEPF Maxwellization.

The divergence of EEPFs in the skin layer of a low frequency ICP can be interpreted as the result of ponderomotive effect caused by the nonlinear Lorentz force $\mathbf{F_L}=en[\mathbf{v}_\omega \times \mathbf{B}_\omega]$. Indeed, since in a cylindrical ICP, $E_{\theta\omega}=-\delta\omega B_{r\omega}$ and, due to the Ramsauer effect and stochastic electron heating, the azimuthal rf electric field $E_{\theta\omega}$ (and so the rf drift velocity $v_{\theta\omega}$) is a weak function of the frequency [42], the ponderomotive force is nearly inversely proportionally to the driving frequency. It has been shown in calculations [43] that the ponderomotive effect is negligibly small at the industrial frequency 13.56 MHz but may be significant at lower frequencies.

The ponderomotive modification of the ambipolar potential U_e and the plasma density n distributions in our ICP operated at 1 mTorr of argon gas, at 0.45 MHz has been demonstrated earlier [33] and is illustrated in Fig. 8. Presented here are the axial distributions of $U_e(z)$ and $n(z)$ at $r=4$ cm and $r=0$; the plasma density was found by integration of the experimental EEPF given in Fig. 4. At low frequency, 0.45 MHz, the distributions are asymmetric relative to the discharge mid plane, and the position z^* of the maximum electron density, and the position z' of minimum ambipolar potential, do not coincide, while at high frequency 6.78 MHz, both distributions are rather symmetrical, with $z^*=z'$, [33]. The shift between z^* and z' in the skin layer at

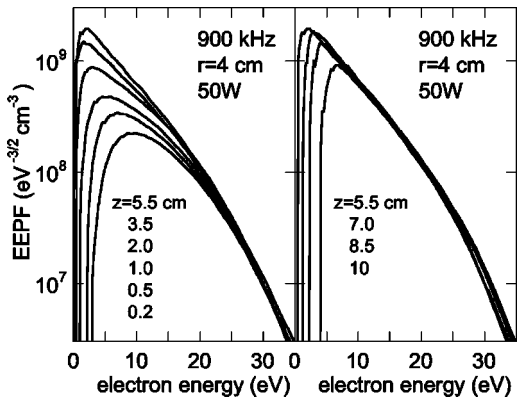

FIG. 7. Axial evolution EEPF at $r=4$ cm for 0.9 MHz, 50 W.

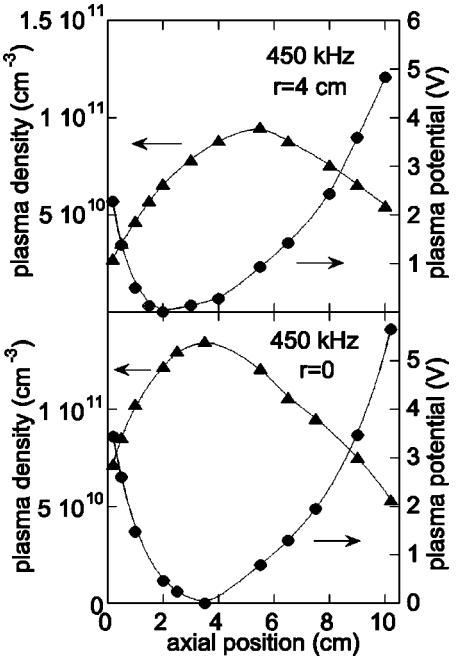

FIG. 8. Plasma density and potential distribution at different radial positions for 0.45 MHz, 1 mTorr, 200 W [33].

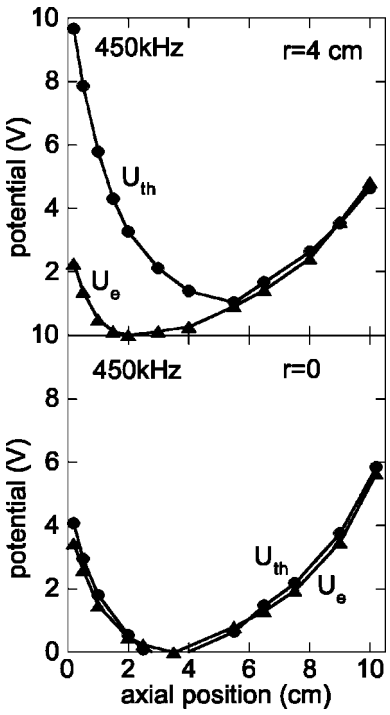

FIG. 9. Plasma thermal and electrical potential at different radial positions for 0.45 MHz, 1 mTorr, 200 W [33].

$r=4$ cm, implies an additional ponderomotive force $F_p = -endU_p/dz$ in the plasma equilibrium balance:

$$T_e\frac{dn}{dz}+en\frac{dU_e}{dz}+en\frac{dU_p}{dz}=0 \tag{1}$$

whose solution is

$$n=n_0\exp(-eU_{th}), \tag{2}$$

where $U_{th}=U_e+U_p=(T_e/e)\ln(n_0/n)$ is the plasma thermal potential. In the absence of the ponderomotive force ($U_p=0$), Eq. (2) reduces to the conventional Boltzmann equilibrium equation ($U_{th}=U_e$). The quantities U_{th} and U_e found in experiment [33] are plotted in Fig. 9 for $r=4$ cm and $r=0$. The disparity between U_{th} and U_e are clearly seen in the skin layer ($r=4$ cm), while far away of skin layer where electromagnetic field is negligibly small, as well as along the discharge axis where $v_{\theta\omega}=0$, the Boltzmann equilibrium is well satisfied ($U_{th}=U_e$). This observation suggests that a considerable ponderomotive effect does exist in our ICP operated at low pressure and low frequency.

According to the main principle of nonlocal electron kinetics, the EEPF in the presence of ponderomotive potential U_p should be a function of the total electron energy including U_p, $f_0(\varepsilon)=f_0(w+U_e+U_p)$. This explains the shift in the energy of the EEPFs measured in the skin layer shown in Figs. 3–5. The change in the shape of EEPFs measured at different positions within the skin layer could be explained by the dependence of U_p on electron kinetic energy and by ponderomotive force acting in the radial direction due to the axial component of the rf magnetic field $B_{z\omega}$ that drives slow electrons (both inwards and outwards) from the position $r=4$ cm corresponding to maximum rf field.

A qualitative explanation of the ponderomotive force effect on the EEPF can be offered as follows. The ponderomotive force in an ICP is mainly the averaged Lorentz force that is proportional to the rf current. Under conditions of the anomalous skin effect, due to thermal electron motion (rf current diffusion), the rf current in the skin layer is smaller than that given by the cold (local) plasma theory. The higher the electron thermal velocity is, the smaller the rf current, and Lorentz force are in the skin layer compared to those given by the local theory. Thus, thermal electron motion reduces the ponderomotive force mainly for slow electrons and therefore EEDF in the skin layer should be depleted of slow electrons.

It is interesting to note that the ponderomotive potential (averaged over electron ensemble) found from Fig. 9 as the difference between U_{th} and U_e appeared to be considerably less than that following from the classical formula for the ponderomotive force derived in the cold plasma (local) approximation. The expression for ponderomotive force in a nonlocal regime ($v_{th}/\delta \gg \omega, \nu_{ea}$) have been obtained in [44], where it has been shown that ponderomotive force in anomalous skin layer is about $v_{th}/\delta\omega$ times smaller than that in the local regime.

IV. THEORY

A straightforward calculation of the electron energy distribution in a cylindrical low pressure, low frequency ICP featuring nonlocal kinetics, nonlocal and nonlinear electrodynamics requires the solution of a spatially inhomogeneous, time-dependent, and multidimensional Boltzmann equation, which is still today a tremendous task. Among the methods

of solving the Boltzmann equation are particle-in-cell (PIC) methods with Monte Carlo collisions [45], deterministic finite difference methods [46], and semianalytical methods [47]. PIC methods suffer from statistical noise and EEPF ''tails'' are rarely shown in PIC simulations. Deterministic methods resolve all points in phase space with equal accuracy. Currently, they require reducing the dimensionality of the problem by using certain approximations. A commonly used approximation is a two-term spherical harmonic expansion in velocity space that reduces the Boltzmann kinetic equation to a Fokker-Planck equation for an isotropic part of the electron velocity distribution function (EVDF) in a four-dimensional space (3D1V). This approach is adequate for the treatment of the majority of electrons in collisional or very high frequency discharges where the EVDF is weakly anisotropic. Both, high frequency and low frequency (or pulsed power) regimes could well be simulated by this method as long as plasma can be adequately described by local electrodynamics when electron current is a local function of the electromagnetic fields. This corresponds to a collision dominated plasma or to a high frequency regime, when $\delta \gg v_{th}/(\nu_{ea}^2+\omega^2)^{1/2}$, (normal skin effect). In this regime of local electrodynamics the isotropic part of the EVDF, f_0 is nonlocal, it is defined by the electric field profiles in the space (around the given point) having scale of the order of electron energy relaxation length, while the anisotropic part of EVDF, $\mathbf{f}_1$ is a local function of electromagnetic field.

For a weakly collisional plasma when $\delta \ll v_{th}/(\nu_{ea}^2+\omega^2)^{1/2}$, (domain of nonlocal electrodynamics, anomalous skin effect), the two-term spherical harmonic expansion is not entirely adequate because it implies a local relationship between electron current and electromagnetic field. However, as long as the field effect may be considered a small perturbation, the EVDF subdivision into a time-independent isotropic part f_0 and a small oscillating anisotropic addition $\mathbf{f}_1$ remains valid. In a weakly collisional warm plasma, the perturbed part of the EVDF, $\mathbf{f}_1$, is also nonlocal, it is strongly affected by the thermal electron motion and depends on field distributions in a vicinity of a given point with dimensions of the order of electron mean free path $\lambda = v_{th}/\nu_{ea}$. The isotropic part f_0 may be found (similarly to that in the local electrodynamics regime) from a spatially averaged kinetic equation and depends solely on the total electron energy. Thus, using this method, the complexity of the problem is reduced to calculation of the perturbed part of the EVDF that in general case still requires solution of a multidimensional kinetic equation. However, for several one-dimensional cases analytical solutions have been obtained and proved to be useful for the analysis of stochastic electron heating, anomalous skin effect, and other warm plasma effects observed recently in weakly collisional ICP discharges.

The traditional perturbation methods are not valid for the EDF treatment in a weakly collisional ICP at low frequency because the perturbed part of the EVDF cannot be considered as a small perturbation. Indeed, with decreasing field frequency, the amplitude of the electron velocity oscillation in the induced electric field may become comparable to or larger than the thermal electron velocity. Moreover, at $\omega < v_\omega/\delta$, the Lorentz force becomes even large than the electric force [33]. Thus, substantial perturbations of the EVDF must be expected and the two-term expansion of the EVDF is no longer valid.

Of primary interest to this paper is the case when the ions do not respond to the field oscillations ($\omega > v_s/\delta \approx 2.3 \times 10^5\ \mathrm{s}^{-1}$), forming a steady positively charged background, whereas the electrons follow the field oscillations. Here $v_s = (T_e/M)^{1/2}$ is the ion sound speed. The Lorentz force in the skin layer produces electron displacement in the direction normal to the plasma boundary (z direction), inducing the polarization electrostatic potential of frequency 2ω with the corresponding electric field in axial direction $E_{z2\omega}$ being much larger than the azimuthal electric field $E_{\theta\omega}$ that maintains the discharge [30]. In a sense, ICPs in this regime resemble capacitively coupled plasmas (CCP) since the electromagnetic force is mainly acting normal to the plasma boundary. A quantitative description of electron kinetics in this regime requires solution of the time-dependent Boltzmann equation in a (2D3V) formulation where the two spatial dimensions are radial and axial position, and the three velocity components are v_θ, v_r, and v_z.

To describe qualitatively the observed depletion of the EEPF by slow electrons in the skin layer, we use the approach developed by Cohen and Rognlien in their calculation of the ponderomotive effect and plasma polarization, caused by the Lorentz force, in a ICP skin layer [48,49]. The main idea of this approach is to utilize exact integrals of the collisionless electron motion and adiabatic invariants to obtain the EVDF in the skin layer from a given EVDF outside the skin layer. They have obtained a one-dimensional analytical solution to the collisionless Boltzmann equation in the skin layer using conservation of the canonical momentum and existence of the longitudinal adiabatic invariant at $v_{th}/\delta\omega \gg 1$. We shall use this solution to describe qualitatively the observed EEPF in a two-dimensional ICP driven by a planar coil.

Consider a planar case when the electromagnetic fields have only B_x and E_y components and the z axis is directed normal to the plasma boundary adjacent to the coil. This case resembles the two-dimensional ICP driven by a planar coil where B_r and E_θ are the main field components in the skin layer. The integral of the particle motion is the canonical momentum $p_y = mv_y - eA_y$, where A_y is the vector magnetic potential. At low frequencies, using conservation of the longitudinal adiabatic invariant, and assuming a Maxwellian EEPF outside the skin layer, one obtains the electron velocity distribution function $f(u_y, u_z, z)$ in the skin layer:

$$f = C \times \begin{cases} \exp(-u_y^2 - u_z^2 - \Phi), & u_z^2 - \Phi + 2u_c u_y - u_c^2 > 0 \\ \exp(-(u_y - u_c)^2 - \Phi), & u_z^2 - \Phi + 2u_c u_y - u_c^2 < 0. \end{cases} \tag{3}$$

Here Φ denotes dimensionless electrostatic potential in the plasma, $\Phi = eU_e/T_e$, and $C = 2n\pi^{-1/2}T_e^{-3/2}$. The upper inequality in Eq. (3) corresponds to free electrons, the lower inequality corresponds to trapped electrons. Here $u = v/v_c$ is a dimensionless velocity, $v_c = eA_y/m$ is the electron oscillatory velocity, and $A_y(z, \phi)$ denotes the value of the vector magnetic potential at a point z at the moment of electron's

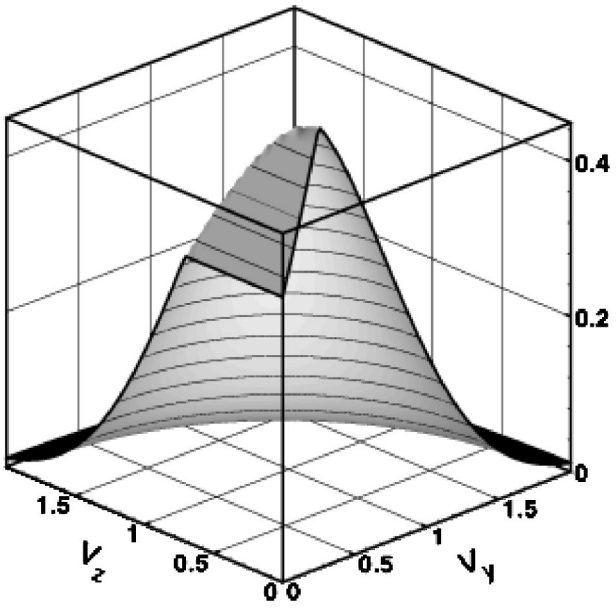

FIG. 10. The EVDF (f/C) given by Eq. 3 for $\Phi(z,\phi)=0$.

reflection by electromagnetic forces. For a sinusoidal wave, $A_y(z,\phi)\propto\sin\phi$. The electrostatic potential Φ has a time-independent (dc) component and a component at 2ω. The oscillating component of Φ builds up to maintain the quasineutrality of the plasma in the skin layer. The ion displacement in the skin layer during the rf period is negligible for an rf field period smaller than the ion transit time through the skin layer. Thus, ions form an immobile background whereas the electrons respond to the instantaneous values of the electromagnetic forces oscillating along the azimuthal direction with frequency ω and in the axial direction with frequency 2ω.

Figure 10 shows the EVDF given by Eq. (3) for $\Phi(z,\phi)=0$. It is seen that the EVDF is depleted with respect to a Maxwellian EVDF at low velocities $u<u_c$. The depletion occurs only in the skin layer and results in an anisotropy (the u_y and u_z velocity components are affected in a different

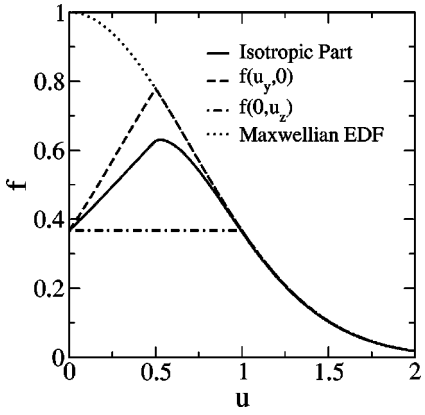

FIG. 11. Instant values of the EVDF in the $u_y=0$ and $u_z=0$ planes, $f(u_z,0,z,\phi)$, and $f(0,u_z,z,\phi)$ at a point z in the skin layer at a moment $t=\phi/\omega$ of maximum amplitude of $A(z,\phi)$, and a result of the EVDF averaging over angle in velocity space $f_0(u,z,\phi)$.

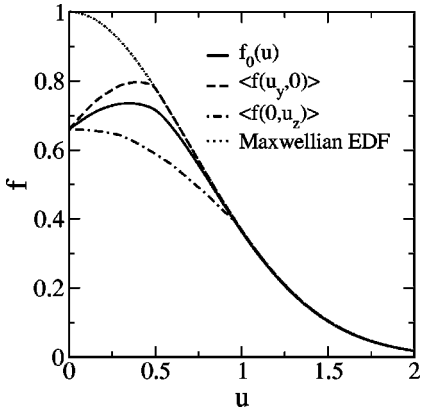

FIG. 12. Averaged over rf period EVDFs in the $u_y=0$ and $u_z=0$ planes and the isotropic part of the EVDF, f_0 obtained by numerical integration of the EVDF given by Eq. (3).

manner) and a time dependency of the EVDF (since the vector magnetic potential A_y oscillates in time). To calculate the time independent isotropic part of the EVDF, f_0 that corresponds to the EEPF, f_0 measured in the experiments, the EVDF given by Eq. (3) was averaged over a rf period and over angle ϕ in the velocity space u_y, u_z. Figures 11 and 12 illustrate the procedure of averaging. Figure 11 shows instantaneous values of the velocity distribution in the $u_y=0$ and $u_z=0$ planes, $f(u_y,0,z,\phi)$ and $f(0,u_z,z,\phi)$ at a point z in the skin layer at a moment $t=\phi/\omega$ of maximum amplitude of $A(z,\phi)$, as well as a result of the EVDF averaging over angle in velocity space $f_0(u,z,\phi)$; Figure 12 shows the velocity distributions in the $u_y=0$ and $u_z=0$ planes, averaged

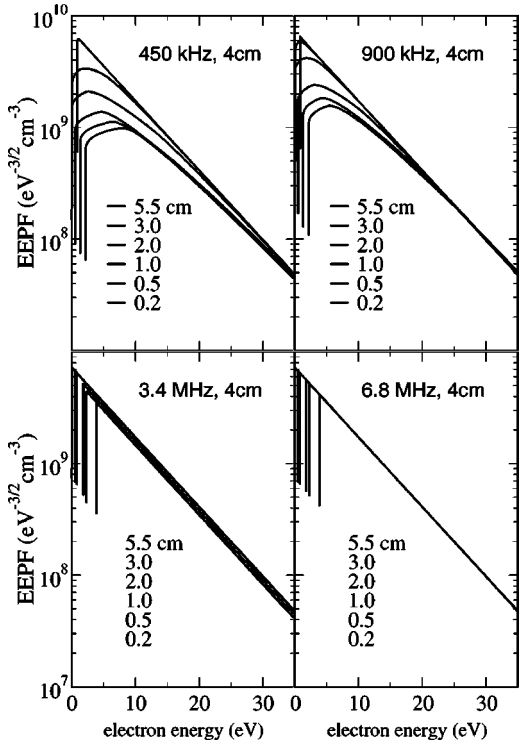

FIG. 13. Calculated EEPFs at different axial positions for frequencies 0.45, 0.9, 3.4, and 6.8 MHz.

over an rf period, as well as the isotropic part of the EVDF, f_0 obtained by numerical integration of the EVDF given by Eq. (3). It is seen that f_0 is depleted at low energy compared to a Maxwellian distribution.

The calculated EEPFs, f_0 for 0.45, 0.9, 3.4, and 6.8 MHz are shown in Fig. 13. The electron density n and temperature T_e used in the calculations, as well as the spatial distributions of the electromagnetic fields $E_{\theta\omega}$, $B_{r\omega}$, and electrostatic potential Φ (dc and oscillating parts) were taken from the experiment [30,33] partly given in Figs. 2 and 8. The experimentally observed distributions of the azimuthal rf electric field and oscillating part of the electrostatic potential were described by the formula

$$E_{\theta\omega}(z) = E_0 \exp(-z/\delta_\omega),$$

$$\Phi_{z2\omega} = \Phi_0 \exp(-z/\delta_{2\omega}),$$

where E_0 and Φ_0 are the azimuthal electric field $E_{\theta\omega}$ and normalized polarization potential $\Phi_{z2\omega}$ at the plasma boundary $(z=0)$, and $\delta_{2\omega}$ is the characteristic decay length for $\Phi_{z2\omega}$.

It is seen from the comparison of the experimental and calculated results that the observed depletion is qualitatively well reproduced by the theory. Different slopes for high energy electrons in the experimental and theoretical EEPFs are due to the assumption (in calculation) of a Maxwellian distribution over the entire electron energy range.

The observed depletion of the EEPF in the skin layer is a result of two effects. The Lorentz force by itself (in the absence of the potential oscillations, $\Phi_{z2\omega}=0$) produces the EEPF depletion in the low energy range starting at velocity u_c. In addition, the Lorentz force results in the oscillating potential $\Phi_{z2\omega}$ that produces a shift of the EEPF as a whole. A rigorous quantitative description of the observed phenomena requires solution of the Boltzmann equation in the 2D3V formulation.

V. CONCLUSIONS

An rf compensated Langmuir probe has been designed for measurement in rf plasmas with large rf field inhomogeneity. Measurements in the skin layer of a low pressure, and low frequency ICP revealed significant EEPF depletion at low electron energy. The depletion was observed only at low frequencies, when conditions of anomalous and nonlinear skin effect are met. The EEPF depletion was interpreted as a ponderomotive effect caused by the Lorentz force affected by electron thermal motion. Under these conditions, the ponderomotive force in the skin layer mainly acts on low energy electrons, thereby depleting the EEPF in this energy range. The EEPF formation under condition of anomalous and nonlinear skin effect was described using a simple analytical theory based on the previous work of Cohen and Rognlien. The EEPF behavior observed in experiment was qualitatively well reproduced by a solution of a collisionless Boltzmann equation accounting for thermal and nonlinear effects due to Lorentz force and the presence of an oscillating polarization potential in the skin layer.

[1] H.U. Eckert, in *Proceedings of the 2nd International Conference on Plasma Chemical Technology*, edited by H.V. Boenig (Techonomic Publishing Company, Pennsylvania, 1986), pp. 171–202.

[2] V.I. Kolobov and V.A. Godyak, IEEE Trans. Plasma Sci. **23**, 503 (1995).

[3] L.D. Tsendin, Plasma Sources Sci. Technol. **4**, 200 (1995).

[4] U. Kortshagen, C. Busch, and L.D. Tsendin, Plasma Sources Sci. Technol. **5**, 1 (1996).

[5] V.A. Godyak and R.B. Piejak, Appl. Phys. Lett. **63**, 3137 (1993).

[6] U. Kortshagen, I. Pukropski, and M. Zethoff, J. Appl. Phys. **76**, 2048 (1994).

[7] V.I. Kolobov, D.F. Beale, L.J. Mahoney, and A.E. Wendt, Appl. Phys. Lett. **65**, 537 (1994).

[8] S.-H. Seo, C-W. Chung, J.-I. Hong, and H.-Y. Chang, Phys. Rev. E **62**, 7155 (2000).

[9] A. Schwabedissen, E.C. Benck, and J.R. Roberts, Phys. Rev. E **55**, 3450 (1997).

[10] A.A. Kudryavtsev and L.D. Tsendin, Tech. Phys. **44**, 1290 (1999).

[11] H. Singh and D.B. Graves, J. Appl. Phys. **87**, 4098 (2000).

[12] G. Mümken, J. Phys. D **32**, 804 (1999).

[13] V.I. Kolobov and D.J. Economou, Plasma Sources Sci. Technol. **6**, R1 (1997).

[14] V.A. Godyak, in *Electron Kinetics in Glow Discharges*, edited by U. Kortshagen and L.D. Tsendin (Plenum Press, New York, 1998), pp. 241–255.

[15] V.A. Godyak, R.B. Piejak, B.M. Alexandrovich, and V.I. Kolobov, Phys. Plasmas **6**, 1804 (1999).

[16] V.I. Kolobov, in *Electron Kinetics in Glow Discharges*, edited by U. Kortshagen and L.D. Tsendin (Plenum Press, New York, 1998), pp. 293–311.

[17] V.A. Godyak and R.B. Piejak, J. Appl. Phys. **82**, 5944 (1997).

[18] M.M. Turner, Phys. Rev. Lett. **71**, 1844 (1993).

[19] V.A. Godyak, R.B. Piejak, and B.M. Alexandrovich, Plasma Sources Sci. Technol. **3**, 169 (1994).

[20] M.A. Lieberman and V.A. Godyak, IEEE Trans. Plasma Sci. **26**, 955 (1998).

[21] V.A. Godyak, R.B. Piejak, B.M. Alexandrovich, and V.I. Kolobov, Phys. Rev. Lett. **80**, 3264 (1998).

[22] V.A. Godyak and V.I. Kolobov, Phys. Rev. Lett. **79**, 4589 (1997).

[23] V.A. Godyak and V.I. Kolobov, Phys. Rev. Lett. **81**, 369 (1998).

[24] H.J. Lee, I.D. Yang, and K.W. Whang, Plasma Sources Sci. Technol. **5**, 383 (1996).

[25] S.S. Kim, Phys. Plasmas **6**, 2926 (1999).

[26] C.-W. Chung, S.-H. Seo, and H.-Y. Chang, Phys. Plasmas **7**, 3584 (2000).

[27] M. Tuszewski, IEEE Trans. Plasma Sci. **27**, 68 (1999).

[28] I.M. El-Fayoumi and I.R. Jones, Plasma Sources Sci. Technol. **6**, 201 (1997).
[29] V.A. Godyak, *in Proceedings of IEEE IAS Annual Meeting, Rome, Italy 2000*, IEEE Conference Record 0-7803-6404-X (IEEE, New York, 2000).
[30] V.A. Godyak, R.B. Piejak, B.M. Alexandrovich, and A.I. Smolyakov, Plasma Sources Sci. Technol. **9**, 541 (2000).
[31] V.A. Godyak, R.B. Piejak, and B.M. Alexandrovich, Phys. Rev. Lett. **83**, 1610 (1999).
[32] V.A. Godyak, in *IEEE International Conference on Plasma Science, New Orleans, 2000*, IEEE Conference Record SB01 (IEEE, New York, 2000), p. 225.
[33] V.A. Godyak, Bulg. J. Phys. **27**, 13 (2000).
[34] V.A. Godyak and R.B. Piejak, J. Appl. Phys. **85**, 703 (1999).
[35] V.A. Godyak, R.B. Piejak, and B.M. Alexandrovich, Plasma Sources Sci. Technol. **1**, 36 (1992).
[36] R.B. Piejak, V.A. Godyak, and B.M. Alexandrovich, J. Appl. Phys. **81**, 3416 (1997).
[37] V.A. Godyak, in *Plasma-Surface Interaction and Processing of Materials*, Vol. 176 of *NATO ASI Series E: Applied Science*, edited by O. Auciello, A. Gras-Marti, J.A. Valles-Abarca, and D. Flamm (Kluwer Academic Press, Dordrecht, 1990), pp. 95–134.
[38] V.A. Godyak and R.B. Piejak, J. Appl. Phys. **68**, 3157 (1990).
[39] V. Vahedi, M.A. Lieberman, G. DiPeso, T.D. Rognlien, and D. Hewett, J. Appl. Phys. **78**, 1446 (1995).
[40] A.I. Smolyakov and I. Khabibrakhmanov, Phys. Rev. Lett. **81**, 4871 (1998).
[41] A. Smolyakov, V. Godyak, and A. Duffy, Phys. Plasmas **7**, 4755 (2000).
[42] V.A. Godyak and R.B. Piejak, J. Appl. Phys. **85**, 3081 (1999).
[43] G. DiPeso, V. Vahedy, D.W. Hewett, and T.D. Rognlien, J. Vac. Sci. Technol. **12**, 1387 (1994).
[44] A.I. Smolyakov, V.A. Godyak, and Yu. Tychetsky (unpublished).
[45] C.K. Birdsall, E. Kawamura, and V. Vahedi, in *Electron Kinetics in Glow Discharges*, edited by U. Kortshagen and L.D. Tsendin (Plenum Press, New York, 1998), pp. 59–74.
[46] V. Batishchev, M.M. Shoucri, A.A. Batishcheva, and I.P. Shkarofsky, J. Plasma Phys. **61**, 347 (1999).
[47] V.I. Kolobov, D.P. Lymberopoulos, and D.J. Economou, Phys. Rev. E **55**, 3408 (1997).
[48] R.H. Cohen and T.D. Rognlien, Plasma Sources Sci. Technol. **5**, 442 (1996).
[49] R.H. Cohen and T.D. Rognlien, Phys. Plasmas **3**, 1839 (1996).